Nano World Journal

https://doi.org/10.17756/nwj.2023-s2-002

Research Article

Open Access

Characterization of Alkali-activated Binder Synthesized from Electric Arc Furnace Slag and Fly Ash

Fatima Ouzoun*, Azzedine Moussadik, Hind Agourrame, Mohamed Saadi and Abdeljebbar Diouri

Laboratory of Applied Materials Chemistry, Faculty of Sciences, Mohammed V University in Rabat, Morocco

***Correspondence to:**
Fatima Ouzoun
Laboratory of Applied Materials Chemistry,
Faculty of Sciences,
Mohammed V University in Rabat, Morocco.
E-mail: fatima.ouzoun@um5r.ac.ma

Received: July 25, 2023
Accepted: September 18, 2023
Published: September 21, 2023

Citation: Ouzoun F, Moussadik A, Agourrame H, Saadi M, Diouri A. 2023. Characterization of Alkali-activated Binder Synthesized from Electric Arc Furnace Slag and Fly Ash. *Nano World J* 9(S2): S6-S11.

Published by United Scientific Group

Abstract

Alkali-activated binders (AABs) have garnered significant interest as promising materials for construction and repair purposes ever since their discovery. They have proven to be environmentally advantageous, causing less pollution compared to conventional cement. These compelling features have made AABs a compelling choice in the realm of construction and repair, offering a sustainable alternative with superior performance. This paper aims to investigate the effect of activator concentration (Sodium hydroxide, NaOH) on AAB composed of electric arc furnace slag (EAFS) and class F fly ash (FA). The study involved a comprehensive analysis conducted over a 28-day curing period at room temperature, utilizing techniques such as X-ray diffraction (XRD), Fourier-transform infrared spectroscopy (FTIR), and thermogravimetric analysis (TG-DTA) to gain a thorough understanding of the developed binders. The results of the study revealed the formation of hydrated phases in the AAB samples. The detected hydrated phases suggest that the activator concentration (NaOH) has a significant impact on the hydration process of AABs.

Keywords

Electric arc furnace slag, Fly ash, Sodium hydroxide concentration, Alkali-activated binders

Introduction

AABs have emerged as a promising alternative to ordinary Portland cement (OPC) due to their excellent mechanical and durability performance, as well as remarkable thermal and fire resistance [1, 2]. These binders are formed by alkali activation of precursors rich in SiO_2 and Al_2O_3, and they offer a wide range of precursor sources. Commonly used precursors for AABs include FA, ground granulated blast furnace slag (GGBFS), metakaolin, and other aluminosilicates [3, 4]. FA and GGBFS, which are industrial waste materials from coal power plants and the steel industry, respectively, are particularly noteworthy as precursors for AABs. FA is known for its pozzolanic properties and is classified as Class C or Class F based on the CaO content [5]. On the other hand, GGBFS exhibits latent hydraulic properties and can hydrate over an extended duration [6]. Both precursors, rich in Si and Al content, contribute to the pozzolanic activity of AABs [3]. The combination of GGBFS and FA in AABs has been found to enhance the matrix strength, leading to improved mechanical performance [1]. The addition of GGBFS increases the formation of calcium aluminosilicate hydrate (C-A-S-H) gels, while FA contributes to the formation of sodium/potassium-aluminosilicate hydrate (N, K)-A-S-H gels, resulting in denser matrices [7, 8]. Moreover, the proportion of slag as a calcium source affects the formation of C-S-H products with certain degrees of aluminum substitution, depending on the availability

of this element in the FA and slag. The activation reactions of slag and FA blended binders are complex, the specific type of gel formed when both precursors are used depends on several factors such as the relative contents of precursors, solution alkalinity, and type of activator [9]. Previous studies have investigated the effect of alkaline activator concentration on the properties of AABs. For instance, Gijbels et al. investigated the effect of NaOH content on alkali/sulfate-activated binders comprising 90 wt.% GGBFS and 10 wt.% phosphogypsum. The molarity of the alkali activator significantly influenced the phase assemblage, with lower molarities (0 M to 1 M) favoring the presence of an amorphous C-S-H phase, while higher molarities (2 M and above) promoted the development of C-A-S-H [10]. Saha and Rajasekaran focused on FA-based geopolymer paste incorporating GGBFS at various percentage levels and different concentrations of NaOH solution. The highest compressive strength achieved was 78.2 MPa for the paste mix with 16 M NaOH solution and 50% GGBFS, indicating that higher dosages of GGBFS facilitated denser structure formation and contributed to increased strength [11]. Ng et al. examined the influence of different NaOH concentrations (6 - 14 M) on FA geopolymers paste and found that the optimal NaOH concentration for forming dense geopolymer samples was determined to be 8 M. Achieving a suitable balance of NaOH is crucial for the substitution of tetrahedral Si with Al, ultimately leading to the highest level of compressive strength [12]. Similarly, Wazien et al. investigated the effects of different NaOH concentrations on the mechanical and morphological properties of a FA-based geopolymer repair material applied on OPC substrate. Optimal results were achieved at a NaOH concentration of 12 M, with compressive strength reaching 92.5 MPa and bond strength measuring 11 MPa at 60 days. The formation of denser material with fewer pores along with the contribution of calcium cations from the OPC substrate surface, were identified as key factors in enhancing the material's strength [13]. From the above literature, it is evident that the synthesis of AABs was highly affected by the type of precursors and concentration of activators. In this study, we focus on the use of EAFS and class F FA as precursor materials for the AABs, and we experimentally analyze the influence of varying molarities of NaOH on the microstructure of the resulting AABs. The synthesized AABs were subjected to 28 days of curing at room temperature, and multiple characterization techniques, including XRD, FTIR, and TG-DTA, are employed to gain insight into the properties of the AABs. The utilization of these precursors not only offers environmental benefits by reducing CO_2 emissions but also facilitates waste recovery.

Materials and Method

Materials

The utilized materials in this study consist of EAFS obtained from the SONASID-Jorf steel plant in Morocco and FA sourced from the Safi thermal power plant. The solid mixture was activated with NaOH. The chemical composition analysis of the EAFS and FA was performed using X-ray fluorescence, and the results are presented in table 1.

Table 1: Chemical composition of EAFS and FA (Wt.%).

Oxides	EAFS	FA
CaO	26.05	1.711
Fe_2O_3	23.33	5.582
SiO_2	10.35	54.63
Al_2O_3	5.95	28.07
MgO	4.68	0.985
SO_3	0.27	0.3566
K_2O	0.05	2.338
TiO_2	0.48	1.711
Na_2O	-	0.3898
MnO	2.77	0.02178
P_2O_5	0.34	0.1672
BaO	-	0.1642
SrO	0.086	0.09227
LOI	24.80	3.7811

Preparation of binders

Two binders were formulated for the study using EAFS and FA. The EAFS and FA were ground to a particle size of 40 µm using the laboratory hammer mill and sieve shaker. Subsequently, the ground EAFS and FA were thoroughly combined and subjected to co-grinding, which involved mechanical activation to enhance the reactivity of the precursors. Following the co-grinding step, the resulting mixture was mixed with two different concentrations of NaOH, namely 4 M and 8 M. The NaOH solutions were prepared by dissolving the appropriate amount of NaOH pellets in distilled water under constant stirring until complete dissolution. The resulting pastes, labeled as F30E70-N4 and F30E70-N8, were placed in a mold. The cast specimens were then subjected to a curing period of 28 days at room temperature. Table 2 presents detailed information on the mass ratios and specific components used in the F30E70-N4 and F30E70-N8 formulations.

Table 2: Mix proportion of the AABs F30E70N4 and F30E70N8 (Wt.%).

Mix	EAFS (Wt.%)	FA (Wt.%)	NaOH (mol/L)	L/S
F30E70N4	70	30	4	0.4
F30E70N8	70	30	8	0.4

Results and Discussion

X-ray diffraction

The mineralogical composition of the raw EAFS and FA samples is displayed in figure 1 and figure 2, respectively. The XRD pattern of the EAFS shows mainly amorphous dispersion peaks, indicating the presence of a glass phase along with some crystalline minerals. The identified mineral phases in the EAFS include Larnite (Ca_2SiO_4), Wuestite (FeO), Fayalite (Fe_2SiO_2), and Olivine ($FeMgSiO_4$). On the other hand, the XRD analysis of the FA sample reveals the presence of crystalline minerals. The dominant crystalline minerals in the FA sample are Mullite ($3Al_2O_3$, $2SiO_2$), Quartz (SiO_2), and Wuestite (FeO).

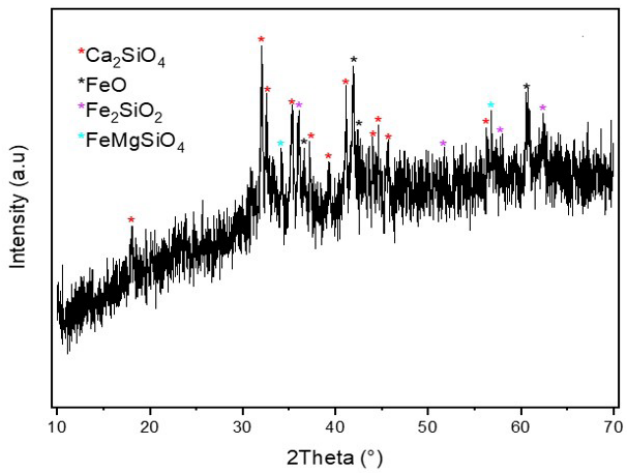

Figure 1: XRD spectra of EAFS: Larnite (Ca_2SiO_4), Wuestite (FeO), Fayalite (Fe_2SiO_2), and Olivine ($FeMgSiO_4$).

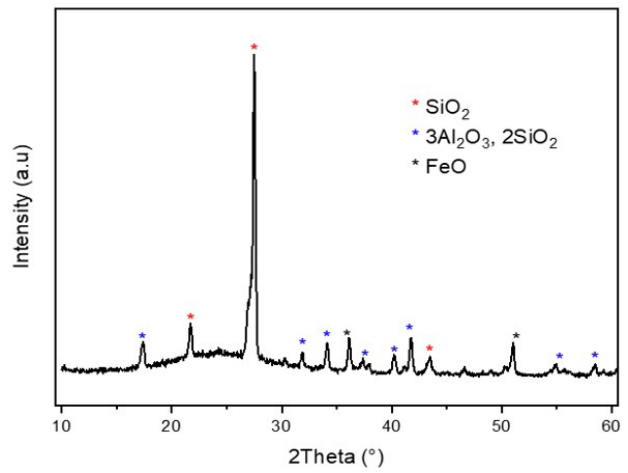

Figure 2: XRD spectra of FA: Mullite ($3Al_2O_3$, $2SiO_2$), Quartz (SiO_2), and Wuestite (FeO).

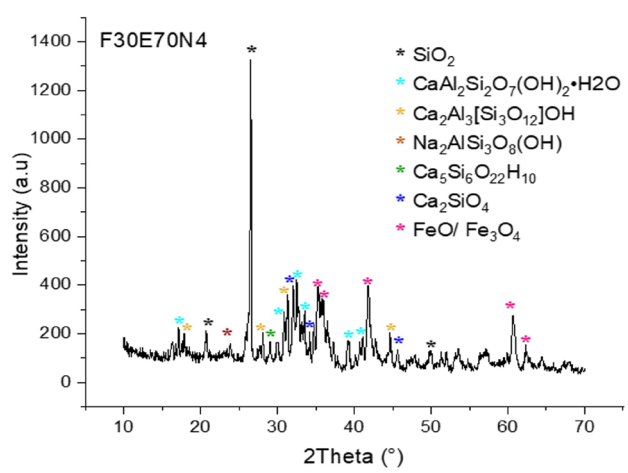

Figure 3: XRD spectra of the AAB F30E70N4 after 28 days of curing: Clinotobermorite ($Ca_5Si_6O_{22}H_{10}$), Lawstonite ($CaAl_2Si_2O_7(OH)_2.H_2O$), Zoisite ($Ca_2Al_3(Si_3O_{12})OH$), Ussingite ($Na_2AlSi_3O_8OH$), Larnite (Ca_2SiO_4), Wustite (FeO), and Magnetite (Fe_3O_4).

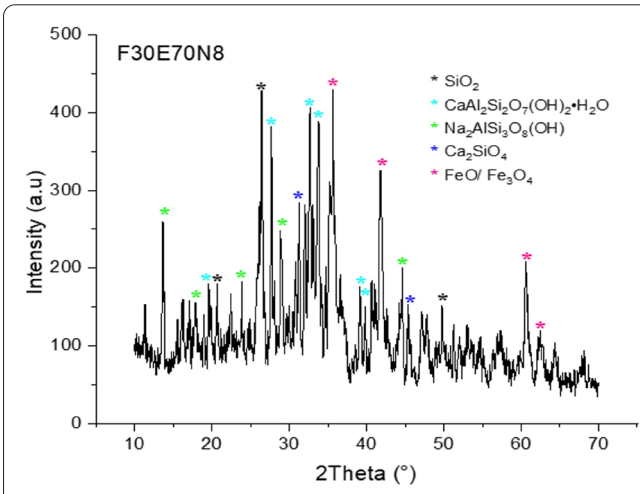

Figure 4: XRD spectra of the AAB F30E70N8 after 28 days of curing: Lawstonite ($CaAl_2Si_2O_7(OH)_2.H_2O$), Ussingite ($Na_2AlSi_3O_8OH$), Larnite (Ca_2SiO_4), Wustite (FeO), and Magnetite (Fe_3O_4).

The X-ray diffractograms of AABs, F30E70N4 and F30E70N8, after 28 days of curing are presented in figure 3 and figure 4, respectively. The analysis of the XRD spectra reveals the presence of silica dioxide (SiO_2) due to the unreacted FA. The presence of CaO in EAFS could have reacted with water leading to the formation of Clinotobermorite phase ($Ca_5Si_6O_{22}H_{10}$) as seen near 29.2° (2θ), it is one of the main products of alkali-activated slag as also reported in the previous study [14]. Other hydration products have been observed including Lawstonite $CaAl_2Si_2O_7(OH)_2.H_2O$, Zoisite $Ca_2Al_3(Si_3O_{12})OH$, and Ussingite ($Na_2AlSi_3O_8OH$). These phases are a result of the reaction between the raw materials and the aqueous alkaline solution. The activated silica and aluminum in EAFS/FA can also be activated by $Ca(OH)_2$ to form C-A-S-H gel. $Ca(OH)_2$ can be produced by the reaction of CaO with water. This explains the chemical bond breaking and recombination of Al-O and Si-O, followed by their combination with Ca^{2+} to produce a new product: C-A-S-H gel (Equations 1 - 3). Peaks corresponding to these phases become more prominent as the molarity of NaOH activator increases from 4 mol/L to 8 mol/L. In alkali activated materials synthesis, the concentration of NaOH in the aqueous phase impacts both the dissolution process and the bonding of solid particles in the final structure [15]. The use of high concentration of NaOH results in enhanced dissolution of the initial solid materials, promoting geopolymerization reactions. As it has been indicated in previous works [16, 17], the alkali-activated FA process evolves through different stages by the dissolution of Si^{4+} and Al^{3+} from coal FA firstly (the high concentration of OH ions in the system is responsible of the breakdown of the Si-O-Si, Si-O-Al and Al-O-Al bonds forming part of the vitreous phase of the ash and therefore of the formation of Si-OH and Al-OH groups). Followed by a condensation step giving place to the precipitation of silicate and aluminate ions where the aluminosilicate gel (N-A-S-H) precipitates. The same conclusion was reached in the case of our study, concerning the structural transformations of FA during alkaline activation. It is obvious from the XRD diagrams of the alkali-activated F30E70N4 and F30E70N8 samples, that as the NaOH concentration in the aqueous phase of the alkali-activated system increases a new crystalline phase is formed. This phase is ascribed to Ussingite ($Na_2AlSi_3O_8OH$). That aligns with the finding of Gao et al. [18], they conducted research on

the effect of NaOH concentration on the SiO_3^{2-} leaching. The findings of this study revealed that with high NaOH concentration, the excess alkali reacts with reactive Al_2O_3 to generate $NaAlO_2$. This compound subsequently interacts with $Na_2O.nSiO_2$, leading to the formation of an insoluble gel composed of sodium aluminosilicate, as illustrated in equation 4 and 5. Based on the study conducted by Sun et al. [19], during alkaline activation of slag, a layer of $Ca(OH)_2$ precipitates may form around the surface of the slag particles as a result of the reaction between the Ca^{2+} in the slag particles and the OH in the solution. In the same context, Marjanović et al. [20] studied the influence of alkali activation conditions on the compressive strengths and the microstructure of alkali-activated FA-blast furnace slag blends. They found that when the concentration of OH^- ions is low, the layer of $Ca(OH)_2$ is not thick enough to impede the diffusion of dissolved Ca^{2+} out of the slag particles. Conversely, when the OH concentration is high, a significant amount of $Ca(OH)_2$ forms around the surface of slag particles, making the diffusion of dissolved Ca^{2+} more challenging. Consequently, there is a reduced availability of Ca^{2+} for reacting with dissolved Si^{4+} and Al^{3+} to form a C-A-S-H gel. In our case, portlandite formation is not detected in the XRD results, which indicates that the concentration we used acts as a catalyst and enhance the dissolution of Si^{4+} and Al^{3+} from FA and slag precursors. There are also more opportunities for incorporation of Na^+ onto the sites usually be filled by Ca^{2+} in C-A-S-H gels derived from (very Ca-rich) EAFS which is in concordance with study of Marjanović et al. [20] and Samantasinghar and Singh [21]. A few peaks of Larnite (Ca_2SiO_4), a mineral in the slag, remain. Additionally, the presence of wustite (FeO) and magnetite (Fe_3O_4) peaks suggests that these phases have not significantly participated in the activation reaction. These XRD results provide valuable insights into the mineralogical transformations and hydration products in the prepared binders, highlighting the effect of activator concentration on the formation of different phases.

$$SiO_2 + OH^- + H_2O \rightarrow [H_3SiO_4]^- \quad (1)$$

$$AlO_2^- + OH^- + H_2O \rightarrow [H_3AlO_4]^{2-} \quad (2)$$

$$[H_3SiO_4]^- + [H_3AlO_4]^{2-} + Ca^{2+} \rightarrow C\text{-}A\text{-}S\text{-}H \quad (3)$$

$$2NaOH + nSiO \rightarrow Na_2O.nSiO_2 + 3H_2O \quad (4)$$

$$Na_2O.nSiO_2 + 2NaAlO_2 + 2H_2O \rightarrow Na_2O.Al_2O_3.nSiO_2.H_2O + 2NaOH \quad (5)$$

FTIR ATR spectroscopy

For the FTIR analysis, the results obtained from the two samples, F30E70N4 and F30E70N8, are identical in terms of their chemical bonds. However, to streamline the interpretation process, only results from sample F30E70N4 are included in this analysis. The FTIR spectra of F30E70N4 sample after 28 days of curing is presented in figure 5. The broad bands located between 2800 and 3700 cm^{-1} and between 1650 - 1694cm^{-1} are characteristics of stretching and deformation vibration of O-H and H-O-H of water molecules, which indicates the presence of hydrated phases as detected on the XRD spectra [22-24]. The bands, at ~995 cm^{-1} and 1067 cm^{-1} correspond to Si-O-Na, Si-O-Si, and Al-O-Si. Thus, the NaOH solution would have separated silica and alumina from FA and

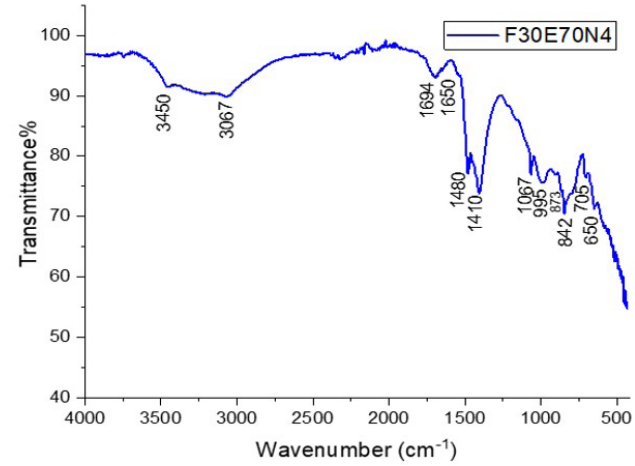

Figure 5: FTIR spectra of AAB F30E70N4 after 28 days of curing.

EAFS, after which Na ions would have reacted and organized with silica and alumina precursors, confirm that multiple gel reaction products are present in alkali-activated sample [25]. Also, it is well known that the (Si-O) vibration in the IR spectra of C-A-S-H and N-A-S-H gels is at 950 - 1100 cm^{-1} [26-28]. Additionally, the adsorption band at about 705 cm^{-1} is attributed to Si-O-Si and Si-O-Al bending modes indicating the main geopolymer structure generated after the reaction between the silicon aluminates and the highly alkali solution and can be found in either C-A-S-H or C-S-H phases. Wustite showed absorption peaks near 873cm^{-1} and 650 cm^{-1} [29, 30]. Peak at 848 cm^{-1} corresponds to the dicalcium silicate phase, remain [31]. The bands in the range of 1400 - 1500 cm^{-1} correspond to O-C-O stretching (carbonates).

Thermal behavior

Thermogram of thermal analysis of AAB (F30E70N4) determined by TG-DTA is shown in figure 6. The measurements are conducted under ambient atmosphere up to a temperature of 900 °C. The TG-DTA curves of the binder exhibit four distinct stages. As observed in the graph, the initial weight loss, which occurs between room temperature and 114 °C, can be attributed to the evaporation of adsorbed water

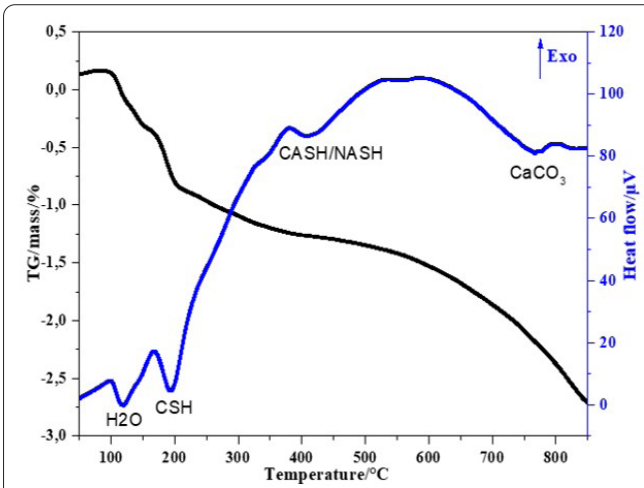

Figure 6: TG-DTA diagram of the AAB F30E70N4 from room temperature to 900 °C.

within the pores of binding gels, which are either (N-A-S-H) type gels or C-(A)-S-H gels [32]. Subsequently, a progressive decomposition of the hydrated gel (C-S-H) takes place, commencing at around 200 °C, along with the evaporation of chemically bonded water within the gel structure [33]. This phenomenon is supported by the presence of an endothermic peak within this temperature range [34]. The water associated is completely removed at 300 °C [1]. The third phase of weight loss, in the range of 300 – 600 °C is attributed to the dehydration of calcium-based reaction products (C-A-S-H, C-(N)-A-S-H) with some Na ions in their structure [35]. Moreover, there is decomposition peak within the range of 300 - 500 °C, which could be related to the dehydroxylation of lawstonite and ussingite. The last loss of weight after 600 °C corresponds to the decomposition of calcite ($CaCO_3$) into CO_2 and CaO [36]. The presence of carbonation products was also identified in FTIR analysis.

Conclusion

In this study, we investigated the alkaline activation of a combination of FA and EAFS using NaOH solution. Our findings indicate that a concentration of 8 M of NaOH promotes the formation of hydrated phases, such as Lawstonite ($CaAl_2Si_2O_7(OH)_2.H_2O$), Clinotobermorite ($Ca_5Si_6O_{22}H_{10}$), and Ussingite ($Na_2AlSi_3O_8OH$). The presence of these hydrated phases plays a substantial role in enhancing the strength and durability of construction materials. The obtained results demonstrate significant potential for utilizing these industrial wastes in the synthesis of AABs. That can be used in the production of ecological concrete, cement-based composites, and other construction products, offering a viable alternative to traditional Portland cement-based materials. This not only reduces industrial waste but also promotes a circular economy within the construction sector. Moving forward, it is recommended to conduct further research focusing on the mechanical properties and long-term durability of these AABs. Exploring their resistance to chemical attack and durability in challenging environmental conditions will facilitate a deeper understanding of their performance in real-world applications.

Acknowledgments

Authors would like to thank ASMENT cement plant and OMRANINNOV-CNRST program (CNRST-HAO-UM5R, number: 573/2021) for their support.

Conflict of Interest

None.

References

1. Rafeet A, Vinai R, Soutsos M, Sha W. 2019. Effects of slag substitution on physical and mechanical properties of fly ash-based alkali activated binders (AABs). *Cement Concr Res* 122: 118-135. https://doi.org/10.1016/j.cemconres.2019.05.003
2. Tayeh BA, Hamada HM, Almeshal I, Bakar BA. 2022. Durability and mechanical properties of cement concrete comprising pozzolanic materials with alkali-activated binder: a comprehensive review. *Case Studies Constr Mater* 17: e01429. https://doi.org/10.1016/j.cscm.2022.e01429
3. Pacheco-Torgal F, Castro-Gomes J, Jalali S. 2008. Alkali-activated binders: a review. Part 2. About materials and binders manufacture. *Constr Build Mater* 22(7): 1315-1322. https://doi.org/10.1016/j.conbuildmat.2007.03.019
4. Li C, Sun H, Li L. 2010. A review: the comparison between alkali-activated slag (Si+Ca) and metakaolin (Si+Al) cements. *Cement Concr Res* 40(9): 1341-1349. https://doi.org/10.1016/j.cemconres.2010.03.020
5. Alterary SS, Marei NH. 2021. Fly ash properties, characterization, and applications: a review. *J King Saud Univ Sci* 33(6): 101536. https://doi.org/10.1016/j.jksus.2021.101536
6. Wan H, Shui Z, Lin Z. 2004. Analysis of geometric characteristics of GGBS particles and their influences on cement properties. *Cement Concr Res* 34(1): 133-137. https://doi.org/10.1016/S0008-8846(03)00252-7
7. Li Z, Liu S. 2007. Influence of slag as additive on compressive strength of fly ash-based geopolymer. *J Mater Civil Eng* 19(6): 470-474. https://doi.org/10.1061/(ASCE)0899-1561(2007)19:6(470)
8. Gao X, Yu QL, Brouwers HJH. 2015. Characterization of alkali activated slag–fly ash blends containing nano-silica. *Constr Build Mater* 98: 397-406. https://doi.org/10.1016/j.conbuildmat.2015.08.086
9. Mohamed OA, Al Khattab R. 2022. Fresh properties and sulfuric acid resistance of sustainable mortar using alkali-activated GGBS/fly ash binder. *Polymers* 14(3): 591. https://doi.org/10.3390/polym14030591
10. Gijbels K, Pontikes Y, Samyn P, Schreurs S, Schroeyers W. 2020. Effect of NaOH content on hydration, mineralogy, porosity and strength in alkali/sulfate-activated binders from ground granulated blast furnace slag and phosphogypsum. *Cement Concr Res* 132: 106054. https://doi.org/10.1016/j.cemconres.2020.106054
11. Saha S, Rajasekaran C. 2017. Enhancement of the properties of fly ash based geopolymer paste by incorporating ground granulated blast furnace slag. *Constr Build Mater* 146: 615-620. https://doi.org/10.1016/j.conbuildmat.2017.04.139
12. Ng HT, Heah CY, Liew YM, Abdullah MMAB. 2018. The effect of various molarities of NaOH solution on fly ash geopolymer paste. *AIP Conf Proc* 2045(1): 020098. https://doi.org/10.1063/1.5080911
13. Zailani AWW, Bouaissi A, Abdullah MMAB, Razak AR, Yoriya S, et al. 2020. Bonding strength characteristics of FA-based geopolymer paste as a repair material when applied on OPC substrate. *Appl Sci* 10(9): 3321. https://doi.org/10.3390/app10093321
14. Naidu TS, Sheridan CM, van Dyk LD. 2020. Basic oxygen furnace slag: review of current and potential uses. *Min Eng* 149: 106234. https://doi.org/10.1016/j.mineng.2020.106234
15. Somna K, Jaturapitakkul C, Kajitvichyanukul P, Chindaprasirt P. 2011. NaOH-activated ground fly ash geopolymer cured at ambient temperature. *Fuel* 90(6): 2118-2124. https://doi.org/10.1016/j.fuel.2011.01.018
16. Panias D, Giannopoulou IP, Perraki T. 2007. Effect of synthesis parameters on the mechanical properties of fly ash-based geopolymers. *Colloids Surf A Physicochem Eng Aspects* 301(1-3): 246-254. https://doi.org/10.1016/j.colsurfa.2006.12.064
17. Palomo Á, Alonso S, Fernandez-Jiménez A, Sobrados I, Sanz J. 2004. Alkaline activation of fly ashes: NMR study of the reaction products. *J Am Ceram Soc* 87(6): 1141-1145. https://doi.org/10.1111/j.1551-2916.2004.01141.x
18. Gao X, Yu QL, Brouwers HJH. 2015. Reaction kinetics, gel character and strength of ambient temperature cured alkali activated slag–fly ash blends. *Constr Build Mater* 80: 105-115. https://doi.org/10.1016/j.conbuildmat.2015.01.065
19. Sun B, Sun Y, Ye G, De Schutter G. 2022. A mix design methodology of slag and fly ash-based alkali-activated paste. *Cement Concr Compos* 126: 104368. https://doi.org/10.1016/j.cemconcomp.2021.104368
20. Marjanović N, Komljenović M, Baščarević Z, Nikolić V, Petrović R. 2015. Physical–mechanical and microstructural properties of alkali-activated fly ash–blast furnace slag blends. *Ceram Int* 41(1): 1421-1435. https://doi.org/10.1016/j.ceramint.2014.09.075

21. Samantasinghar S, Singh SP. 2019. Fresh and hardened properties of fly ash–slag blended geopolymer paste and mortar. *Int J Concr Struct Mater* 13: 47. https://doi.org/10.1186/s40069-019-0360-1

22. Ismail I, Bernal SA, Provis JL, Hamdan S, van Deventer JS. 2013. Microstructural changes in alkali activated fly ash/slag geopolymers with sulfate exposure. *Mater Struct* 46: 361-373. https://doi.org/10.1617/s11527-012-9906-2

23. Djobo JNY, Elimbi A, Tchakouté HK, Kumar S. 2016. Reactivity of volcanic ash in alkaline medium, microstructural and strength characteristics of resulting geopolymers under different synthesis conditions. *J Mater Sci* 51: 10301-10317. https://doi.org/10.1007/s10853-016-0257-1

24. Djon Li Ndjock BI, Baenla J, Mbah JBB, Elimbi A, Cyr M. 2020. Amorphous phase of volcanic ash and microstructure of cement product obtained from phosphoric acid activation. *SN Appl Sci* 2: 720. https://doi.org/10.1007/s42452-020-2496-7

25. Ahmad MR, Das CS, Khan M, Dai JG. 2023. Development of low-carbon alkali-activated materials solely activated by flue gas residues (FGR) waste from incineration plants. *J Clean Prod* 397: 136597. https://doi.org/10.1016/j.jclepro.2023.136597

26. García-Lodeiro I, Palomo A, Fernández-Jiménez A, Macphee DE. 2011. Compatibility studies between NASH and CASH gels. Study in the ternary diagram Na_2O-CaO-Al_2O_3-SiO_2-H_2O. *Cement Concr Res* 41(9): 923-931. https://doi.org/10.1016/j.cemconres.2011.05.006

27. Walkley B, San Nicolas R, Sani MA, Rees GJ, Hanna JV, et al. 2016. Phase evolution of C-(N)-ASH/NASH gel blends investigated via alkali-activation of synthetic calcium aluminosilicate precursors. *Cement Concr Res* 89: 120-135. https://doi.org/10.1016/j.cemconres.2016.08.010

28. Onutai S, Osugi T, Sone T. 2023. Alumino-silicate structural formation during alkali-activation of metakaolin: in-situ and ex-situ ATR-FTIR studies. *Materials* 16(3): 985. https://doi.org/10.3390/ma16030985

29. Chukanov NV. 2013. Infrared Spectra of Mineral Species: Extended Library. Springer Dordrecht.

30. Agarwal DK, Palayil JK. 2022. Recovery of hydrothermal wustite-magnetite spherules from the Central Indian Ridge, Indian Ocean. *Sci Rep* 12(1): 6811. https://doi.org/10.1038/s41598-022-10756-1

31. Salman M, Cizer Ö, Pontikes Y, Snellings R, Dijkman J, et al. 2015. Alkali activation of AOD stainless steel slag under steam curing conditions. *J Am Ceram Soc* 98(10): 3062-3074. https://doi.org/10.1111/jace.13776

32. Gao Y, Huang H, Tang W, Liu X, Yang X, et al. 2015. Preparation and characterization of a novel porous silicate material from coal gangue. *Microporous Mesoporous Mater* 217: 210-218. https://doi.org/10.1016/j.micromeso.2015.06.033

33. Qin L, Gao X. 2019. Properties of coal gangue-Portland cement mixture with carbonation. *Fuel* 245: 1-12. https://doi.org/10.1016/j.fuel.2019.02.067

34. Alarcon-Ruiz L, Platret G, Massieu E, Ehrlacher A. 2005. The use of thermal analysis in assessing the effect of temperature on a cement paste. *Cement Concr Res* 35(3): 609-613. https://doi.org/10.1016/j.cemconres.2004.06.015

35. Ahmad MR, Das CS, Khan M, Dai JG. 2023. Development of low-carbon alkali-activated materials solely activated by flue gas residues (FGR) waste from incineration plants. *J Clean Prod* 397: 136597. https://doi.org/10.1016/j.jclepro.2023.136597

36. Khan MZN, Hao Y, Hao H. 2016. Synthesis of high strength ambient cured geopolymer composite by using low calcium fly ash. *Constr Build Mater* 125: 809-820. https://doi.org/10.1016/j.conbuildmat.2016.08.097